

On the Nonlinear Dynamics of Pursuit Guidance for Marine Vehicles

Fotis A. Papoulias¹

A theoretical analysis of the nonlinear dynamic phenomena involved in pure pursuit guidance of marine vehicles is performed. Nomoto's model (Crane et al 1989) is used to provide the basis for the main vehicle turning lag. Results obtained in closed-form expressions demonstrate the existence of bifurcations to periodic solutions. The center manifold of the system is evaluated to within a third-order approximation. Third- and fifth-order expansions are utilized in order to provide information on limit cycle existence and stability. Recommendations regarding the appropriate selection of control design parameters are provided.

Introduction

SOFTWARE organization of a marine vehicle under automatic path control consists of a number of dynamical systems which, besides having their own specific response characteristics, exchange information and interact with each other (Byrnes et al 1992). At the heart of the vehicle software there exist three mutually interacting loops, namely navigation, guidance, and control (Healey et al 1990), as is schematically depicted in Fig. 1. The navigation loop processes positional information, determines the actual geographical location of the vehicle and compares it to the commanded path which is generated by the path planning operations. This loop has its own dynamics but it operates at a rather slow rate since the mission requirements usually vary slowly compared to the vehicle dynamics. The guidance loop accepts navigational information and generates appropriate commands which in turn become the input to the vehicle autopilot systems, and these determine the necessary vehicle actuator signals. For accurate path keeping, the guidance and autopilot functions have similar dynamic response characteristics and this may create stability problems once the two systems are coupled together (Papoulias 1993a). In this work we concentrate on the analytical aspects of the loss of stability of straight line motion in the case of orientation control and pursuit guidance laws. In this scheme, the guidance law commands a heading angle which the autopilot is called upon to deliver. The initial loss of stability is evaluated analytically in terms of the autopilot damping ratio and natural frequency, and the guidance preview distance. Curved path, positional time lag, and hydrostatic restoring moment effects on stability are also analyzed. Nonlinear analysis and bifurcation theory (Guckenheimer & Holmes 1983) techniques are utilized in order to assess the dynamics of the system after loss of stability. We use a third-order expansion in the equations of motion to reduce the system to an equivalent second-order model. The method of averaging (Chow & Mallet-Paret 1977) is utilized to predict the existence and stability properties of the resulting periodic solutions. Techniques based on the formulas presented in Hassard & Wan (1978) gave identical results with the

ones obtained here. The existence of supercritical and subcritical Poincaré-Andronov-Hopf (PAH) bifurcations is further analyzed via fifth-order approximations of the equations of motion and consistent center manifold reductions. The results reveal the existence of double limit cycles, one stable and one unstable, with significant consequences on the domain of attraction of straight line motion. An unstable limit cycle reduces the stability domain considerably before the nominal level flight path becomes unstable. It is shown that this situation is directly related to the amount of damping selected in the autopilot design. All computations in this work are performed for the Naval Postgraduate School test-bed autonomous vehicle for which a fairly accurate set of hydrodynamic coefficients and geometric properties is available (Warner 1991, Bahrke 1992). All results are presented in standard dimensionless form by nondimensionalizing with respect to the vehicle length and forward speed.

1. Problem formulation

In this section we introduce the vehicle equations of motion and their simplification which leads to the design of a heading autopilot. The guidance law which is used to provide path keeping along straight line segments is then presented.

Model reduction

The maneuvering equations of motion of an ocean vehicle in the horizontal plane are written in dimensionless form as

$$m(\dot{v} + r + x_G r) = Y_r \dot{r} + Y_v \dot{v} + Y_r r + Y_v v + Y_\delta \delta_s + Y_{\delta_b} \delta_b - \int_{\text{tail}}^{\text{nose}} C_D h(\xi)(v + \xi r)|v + \xi r| d\xi \quad (1)$$

$$I_z \dot{r} + m x_G (\dot{v} + r) = N_r \dot{r} + N_v \dot{v} + N_r r + N_v v + N_\delta \delta_s + N_{\delta_b} \delta_b - \int_{\text{tail}}^{\text{nose}} C_D h(\xi)(v + \xi r)|v + \xi r| \xi d\xi \quad (2)$$

where only the coefficients that have nonzero values in the present model have been kept and the symbols are explained in the Nomenclature. The cross flow integral drag terms in the equations of motion become very important for hovering operations or low-speed maneuvering, whereas at higher for-

¹Assistant professor, Department of Mechanical Engineering, Naval Postgraduate School, Monterey, California.

Manuscript received at SNAME headquarters May 7, 1992; revised manuscript received November 5, 1992.

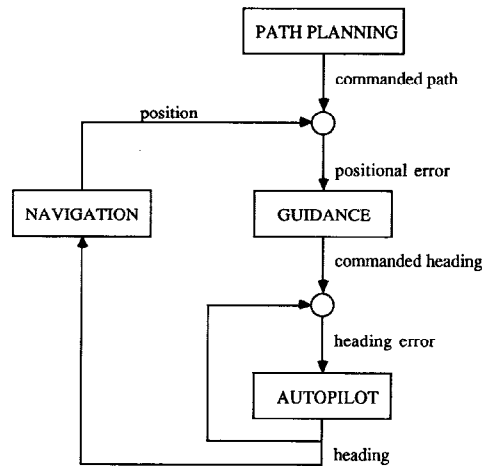


Fig. 1 Navigation, guidance, and control system diagram

ward speeds the angle of attack with respect to the water becomes progressively smaller and the steering response is predominantly linear. Furthermore, for maximum maneuverability, the vehicle bow rudder is deflected at the same amount and opposite to the stern rudder; i.e., $\delta = \delta_s = -\delta_b$. Although some moderate bow rudder stall has been observed in tight turning experiments, there has been no need for separate rudder control thus far.

In this way the linearized equations of motion (1) and (2) are written in the form

$$\dot{v} = a_{11}v + a_{12}r + b_1\delta \quad (3)$$

$$\dot{r} = a_{21}v + a_{22}r + b_2\delta \quad (4)$$

where

$$Da_{11} = (I_z - N_r)Y_v - (mx_G - Y_r)N_v$$

$$Da_{12} = (I_z - N_r)(Y_r - m) - (mx_G - Y_r)(N_r - mx_G)$$

$$Da_{21} = (m - Y_v)N_v - (mx_G - N_v)Y_v$$

$$Da_{22} = (m - Y_v)(N_r - mx_G) - (mx_G - N_v)(Y_r - m)$$

$$Db_1 = (I_z - N_r)(Y_{\delta_s} - Y_{\delta_b}) - (mx_G - Y_r)(N_{\delta_s} - N_{\delta_b})$$

$$Db_2 = (m - Y_v)(N_{\delta_s} - N_{\delta_b}) - (mx_G - N_v)(Y_{\delta_s} - Y_{\delta_b})$$

$$D = (I_z - N_r)(m - Y_v) - (mx_G - Y_r)(mx_G - N_v)$$

The transfer function between rudder angle δ and turning rate r is obtained from equations (3) and (4) as

$$\frac{r}{\delta} = \frac{b_2s + (a_{21}b_1 - a_{11}b_2)}{s^2 - (a_{11} + a_{22})s + (a_{11}a_{22} - a_{12}a_{21})} \quad (5)$$

This second-order transfer function can be simplified for low-frequency maneuvering motions by rewriting it as δ/r , expanding in Taylor series in s , and keeping the first-order terms only. This procedure yields

$$\frac{r}{\delta} = \frac{b}{s - a} \quad \text{or} \quad \dot{r} = ar + b\delta \quad (6)$$

where

$$a = \frac{(a_{11}a_{22} - a_{12}a_{21})(a_{21}b_1 - a_{11}b_2)}{(a_{11} + a_{22})(a_{21}b_1 - a_{11}b_2) + b_2(a_{11}a_{22} - a_{12}a_{21})}$$

$$b = \frac{(a_{21}b_1 - a_{11}b_2)^2}{(a_{11} + a_{22})(a_{21}b_1 - a_{11}b_2) + b_2(a_{11}a_{22} - a_{12}a_{21})}$$

Equation (6), which is sometimes called Nomoto's first-order model, captures the fundamental characteristics of vehicle turning and is particularly useful in control system design since no sway velocity feedback is necessary. For auto-

Nomenclature

a = dummy independent variable, or yaw rate coefficient in Nomoto's model
 a_1 = equivalent spring restoring moment coefficient
 A = linearized system matrix
 b = rudder angle coefficient in Nomoto's model
 C_D = drag coefficient
 d = guidance law preview distance
 d_{crit} = critical value of d for stability
 $d_{crit}^{R_1}$ = value of d_{crit} for a curved reference path
GPS = Global Positional System
 I_z = vehicle mass moment of inertia
INS = Inertial Navigational System
 \mathcal{H} = cubic stability coefficient
 k_1, k_2 = controller gains
 \mathcal{L} = quintic stability coefficient
 m = vehicle mass
 N = yaw moment
 N_a = derivative of N with respect to a
PAH = Poincare-Andronov-Hopf bifurcation

r = yaw rate
 R = radius of curvature of nominal path, or polar coordinate of transformed reduced system
 t = time
 T = matrix of eigenvectors of A
 T = limit cycle period, or positional information time lag
 v = sway velocity
 \mathbf{x} = state variables vector
 x_G = body fixed coordinate of vehicle center of gravity
 y = deviation off commanded path
 Y = sway force
 Y_a = derivative of Y with respect to a
 \mathbf{z} = state variables vector in canonical form
 z_1, z_2 = critical variables of \mathbf{z}
 z_3 = stable coordinate of \mathbf{z}

Greek symbols

α = real part of critical pair of eigenvalues

α' = derivative of α with respect to d evaluated at d_{crit}
 α_i = coefficients in center manifold expansion of z_3
 β = Floquet exponent of limit cycles
 δ, δ_s = stern rudder angle
 δ_b = bow rudder angle
 δ_0 = linearized rudder angle control law
 δ_{sat} = saturation level of rudder angle
 ϵ = criticality difference $d - d_{crit}$
 ζ = damping ratio of heading angle
 ζ_{crit} = critical value of ζ for limit cycle stability
 θ = polar coordinate of transformed reduced system
 ψ = vehicle heading angle
 ψ_c = commanded heading angle
 ω_n = natural frequency of heading response
 ω = imaginary part of critical pair of eigenvalues
 ω' = derivative of ω with respect to d evaluated at d_{crit}

mous vehicles where space is at a premium this is important because it eliminates the need for side slip angle sensors.

Control law

A linear heading feedback control law based on equation (6) has the form

$$\delta_0 = k_1(\psi - \psi_c) + k_2 r \quad (7)$$

where ψ_c is the commanded heading angle. The system characteristic equation is obtained from (6), (7), and

$$\dot{\psi} = r \quad (8)$$

as

$$s^2 - (a + bk_2)s - bk_1 = 0 \quad (9)$$

If the desired characteristic equation is

$$s^2 + 2\zeta\omega_n s + \omega_n^2 = 0 \quad (10)$$

the controller gains are computed from

$$k_1 = -\frac{\omega_n^2}{b} \quad (11)$$

$$k_2 = -\frac{a + 2\zeta\omega_n}{b} \quad (12)$$

The natural frequency ω_n and damping ratio ζ are selected based on general guidelines for second-order system transient response (Friedland 1986). In order to capture the effect of rudder saturation, the commanded rudder angle is given by

$$\delta = \delta_{\text{sat}} \tanh\left(\frac{\delta_0}{\delta_{\text{sat}}}\right) \quad (13)$$

where δ_0 is the slope of δ at the origin given by (7), and δ_{sat} is the saturation limit on δ typically set at 0.4 radians. The hyperbolic tangent function (13) is used instead of a hard saturation function because of its analyticity properties. Furthermore, the time response of the system remains effectively the same regardless of which function is actually used. What is important is the slope of the function at zero δ_0 , and the actual saturation limit δ_{sat} .

Guidance scheme

Since the previous control law stabilizes the vehicle to any commanded heading angle, it must be coupled with an appropriate orientation guidance law to provide path keeping and path changing capabilities. Unlike the autopilot which is based on the vehicle turning rate lag (6) and heading rate (8), the guidance law is based on the inertial deviation rate from the commanded path

$$\dot{y} = \sin \psi \quad (14)$$

The simplest orientation guidance law is pure pursuit guidance accomplished as illustrated in Fig. 2. The vehicle is located at (x, y) and attempts to point its longitudinal axis towards a target point D located ahead of the vehicle at a constant preview distance d on the nominal straight line path. Pure pursuit guidance is achieved by commanding a heading angle ψ_c equal to the line of sight angle σ ,

$$\psi_c = -\tan^{-1} \frac{y}{d} \quad (15)$$

It can be easily seen (Papoulias 1993b) that if the vehicle were infinitely responsive, in other words if $\psi_c = \psi$, the above guidance law would be globally asymptotically stable. Smaller values of the preview distance d result in faster guidance

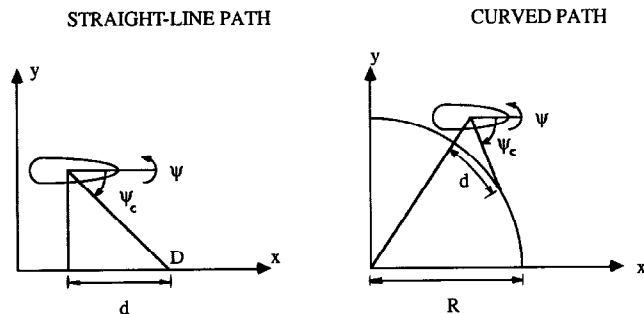


Fig. 2 Vehicle geometry and definitions of symbols

law response. On the other hand, the autopilot has a limited reaction time according to the specified natural frequency ω_n and damping ratio ζ , the vehicle natural time constant $-1/a$, and the actuator strength b . For this reason, stability of the combined guidance and control scheme is no longer guaranteed and the problem then becomes how to assess the dynamic response of the system in the (d, ζ, ω_n) parameter space.

2. Loss of stability

Although the control law guarantees stability for a constant commanded heading angle ψ_c , this is no longer the case when ψ_c is a function of the vehicle response through the guidance law (15). In this section we analyze the linear stability properties of the trivial equilibrium solution characterized by

$$\psi = r = y = 0 \quad (16)$$

which corresponds to straight line motion at the commanded path.

Critical preview distance

The complete system is given by

$$\begin{aligned} \dot{\psi} &= r \\ \dot{r} &= ar + b\delta_{\text{sat}} \tanh\left\{\frac{1}{\delta_{\text{sat}}}\left[k_1\left(\psi + \tan^{-1}\frac{y}{d}\right) + k_2 r\right]\right\} \end{aligned} \quad (17)$$

$$\dot{y} = \sin \psi$$

or in compact form

$$\dot{\mathbf{x}} = \mathbf{f}(\mathbf{x}), \quad \mathbf{x} = [\psi, r, y]^T \quad (18)$$

It can be easily seen that (16) is the only equilibrium state of (18), so that no steady-state bifurcations are expected here unlike the vertical plane case (Papoulias 1992b). Linearization of equations (18) in the vicinity of (16) produces the linear system

$$\dot{\mathbf{x}} = \mathbf{A}\mathbf{x} \quad (19)$$

where \mathbf{A} is the Jacobian matrix of $\mathbf{f}(\mathbf{x})$

$$\mathbf{A} = \begin{bmatrix} 0 & 1 & 0 \\ bk_1 & a + bk_2 & \frac{bk_1}{d} \\ 1 & 0 & 0 \end{bmatrix} \quad (20)$$

Local stability properties of (16) are then established by the eigenvalues of (20). Writing out the characteristic equation of \mathbf{A} we get

$$-\lambda^3 + (a + bk_2)\lambda^2 + bk_1\lambda + \frac{bk_1}{d} = 0 \quad (21)$$

It can be seen that in the absence of guidance law ($d \rightarrow \infty$), the dynamics of (21) reduce to the dynamics selected from the control law design through the desired characteristic equation (10), with the additional pole at the origin corresponding to $y = \text{const}$.

Applying Routh's criterion to the cubic (21) we get

$$(a + bk_2)bk_1 + \frac{bk_1}{d} = 0$$

from which the critical preview distance is determined as

$$d_{\text{crit}} = \frac{1}{2\zeta\omega_n} \quad (22)$$

For $d > d_{\text{crit}}$ all roots of (21) have negative real parts which means that the combined guidance and control law provides asymptotic stability for (16). Although no other equilibrium states exist, the above asymptotic stability is not necessarily global, as other attractors such as limit cycles may exist in the state space. Existence and stability of these limit cycles are analyzed in Section 3.

Interpretation

The loss of stability of the guidance and control scheme is explained as follows: For $d < d_{\text{crit}}$ the guidance law has dynamics faster than the autopilot closed loop dynamics and as a result the control law is inadequate in following the commanded heading angle. It is the fact that this commanded heading is obtained through the intermediate closed loop depicted in Fig. 1 which results in a loss of stability. If the commanded heading were a (possibly rapidly varying) function of time only, a sufficiently high bandwidth controller should guarantee both stability and reasonable steady-state accuracy.

To arrive at a physical interpretation of the critical preview distance, consider the equations of motion (6), (8), and (14), along with a simplified control law of the form $\delta = k(\psi - \psi_c)$. It can be easily seen that any negative value of the gain k guarantees heading control stability. When ψ_c is given by (15) the critical value d_{crit} is

$$d_{\text{crit}} = -\frac{1}{a} \quad (23)$$

The ratio $-1/a$ is the time constant of the vehicle turning dynamics, whereas d is the inverse time constant of the guidance law from (14) and (15). It follows then that loss of stability occurs when the time constant of the guidance law is smaller than the time constant of the vehicle dynamics.

It should be emphasized that this loss of stability is entirely due to the interaction of guidance and control dynamics and not due to the use of a linear controller for a nonlinear system. Indeed, the nonlinear steering model is

$$\begin{aligned} \dot{\psi} &= r \\ \dot{r} &= ar + cr^3 + b\delta_{\text{sat}} \tanh \frac{k\psi}{\delta_{\text{sat}}} \end{aligned}$$

where both rudder saturation and nonlinear ($r - \delta$) dynamics have been included. We have already seen that $k < 0$ guarantees stability through linearization. To show stability for the nonlinear system consider the Lyapunov function

$$V = -\frac{r^2}{2a} - \frac{b\delta_{\text{sat}}^2}{k} \ln \left(\cosh \frac{k\psi}{\delta_{\text{sat}}} \right)$$

which is simply the sum of the kinetic

$$-\frac{r^2}{2a}$$

and the potential energy

$$-b\delta_{\text{sat}} \int \tanh \frac{k\psi}{\delta_{\text{sat}}} d\psi$$

The time derivative of V is

$$\dot{V} = -r^2 - \frac{c}{a}r^4 < 0$$

for every $(\psi, r) \neq (0, 0)$ except on the ψ -axis. Still, in such a case V can be slightly modified such that V is negative definite for all $(\psi, r) \neq (0, 0)$ (Guckenheimer & Holmes 1983).

Curvature effects

For obstacle avoidance and terrain following tasks, it is necessary that the vehicle must be able to follow a curved reference path. Without loss of generality we can assume that the curved path is discretized into a series of circular paths with constant radius of curvature R (Papoulias 1991), Fig. 2. The control law is written as

$$\delta = k_1(\psi - \psi_c) + k_2r + k_0 \quad (24)$$

where the feedforward term k_0 is used to guarantee steady-state path accuracy and the feedforward terms k_1, k_2 are the same as before since the linearized vehicle turning dynamics do not change significantly from the nominal straight-line motion case. The commanded heading angle in (24) is the line of sight angle (Papoulias 1991)

$$\tan \psi_c = \frac{y(x^2 + y^2)^{1/2} - R[y \cos(d/R) - x \sin(d/R)]}{x(x^2 + y^2)^{1/2} - R[x \cos(d/R) + y \sin(d/R)]} \quad (25)$$

At steady state the vehicle assumes a turning rate $r_s = 1/R$, and $x_s = R \cos(r_s t)$, $y_s = R \sin(r_s t)$ where we have assumed that the steady-state cross track error deviation from the circular path is zero. Substituting into (25) we get

$$(\psi_c)_s = \tan^{-1} \left(\frac{\sin(d/R)}{1 - \cos(d/R)} \right) + \frac{1}{R} t$$

The steady-state control effort is then determined by

$$-k_1 \tan^{-1} \left(\frac{\sin(d/R)}{1 - \cos(d/R)} \right) + \frac{k_2}{R} + k_0 = -\frac{a}{b} \frac{1}{R} \quad (26)$$

where the left-hand side is obtained from (24), and the right-hand side from the equation of motion $\dot{r} = ar + b\delta$. Equation (26) can be used to evaluate the appropriate feedforward term k_0 .

If we introduce a coordinate frame moving along the above circular path with the vehicle at steady state, the equations of motion become

$$\begin{aligned} \dot{\psi}_1 &= r_1 \\ \dot{r}_1 &= ar_1 + b\delta_1, \quad \delta_1 = k_1(\psi_1 - \sigma_1) + k_2r_1, \quad \sigma_1 = \gamma - \gamma_0 \\ \dot{y}'_1 &= \sin \psi_1 \end{aligned} \quad (27)$$

where

$$\tan \gamma_0 = \frac{\sin(d/R)}{1 - \cos(d/R)}, \quad \tan \gamma = \frac{R \sin(d/R)}{R + y'_1 - R \cos(d/R)} \quad (28)$$

subscript 1 corresponds to the state variables in the moving reference frame, and $y'_1 = (x^2 + y^2)^{1/2} - R$ is the cross track

error off the circular path. Loss of stability of (27) and (28) occurs at

$$d_{\text{crit}}^{(R)} = 2R \tan^{-1} \left(\frac{d_{\text{crit}}}{2R} \right) \quad (29)$$

where $d_{\text{crit}} = 1/2\zeta\omega_n$ is the critical preview distance for a straight line path, $R \rightarrow \infty$. Equation (29) shows that

$$d_{\text{crit}}^{(R)} < d_{\text{crit}} \quad (30)$$

in other words, a stable guidance and control law for straight line segments will guarantee stability along curved paths as well. This result was observed numerically in Papoulias (1991).

Time lag effects

Implementation of the previously developed guidance and control law requires inertial position information at the same rate as heading angle and turning rate. In the confined space of an autonomous vehicle where accurate Inertial Navigational System (INS) cannot be installed, position estimation can be achieved by an improved dead reckoning scheme (Warner 1991), the incorporation of Global Positional System (GPS) and INS (Kwak et al 1992), and the use of the vehicle sonars (Brutzman 1992). Dead reckoning provides an estimate of position only and it cannot recover the true vehicle position. This is accomplished by GPS/INS and sonar data but at a slower rate than the autopilot functions, due to surfacing requirements for GPS and the significant sonar data analysis and reduction required. To analyze the stability effects of such positional information lags we write the linearized system of equations in the form

$$\begin{aligned} \dot{\psi} &= r \\ \dot{r} &= -\omega_n^2 \psi - 2\zeta\omega_n r - \frac{\omega_n^2}{d} y(t-T) \\ \dot{y} &= \psi \end{aligned} \quad (31)$$

where T is the time lag.

The characteristic equation of (31) is

$$s^3 + 2\zeta\omega_n s^2 + \omega_n^2 s + \frac{\omega_n^2}{d} e^{-Ts} = 0 \quad (32)$$

A first estimate of the critical preview distance d for stability of (32) can be found by using the approximation $e^{-Ts} = 1 - Ts$. In such a case, d must satisfy the condition

$$d > \frac{1}{2\zeta\omega_n} + T \quad (33)$$

and it can be seen that a nonzero T may result in a significant enlargement of the region of instability.

The exact value of d for stability can be computed by recasting (32) in the form

$$1 + \frac{1}{d} \frac{\omega_n^2 e^{-Ts}}{s(s^2 + 2\zeta\omega_n s + \omega_n^2)} = 0 \quad (34)$$

The magnitude and phase angle of the open-loop transfer function of (34) are

$$|G(i\omega)| = \frac{\omega_n^2}{\omega d \sqrt{(-\omega^2 + \omega_n^2)^2 + (2\zeta\omega\omega_n)^2}} \quad (35)$$

$$\phi = -\frac{1}{2}\pi - \omega T - \tan^{-1} \left(\frac{2\zeta\omega\omega_n}{-\omega^2 + \omega_n^2} \right) \quad (36)$$

The phase crossover frequency ω_1 is the value of ω such that $\phi = -\pi$. Using (36) this is computed from

$$\omega_n^2 - \omega_1^2 - 2\zeta\omega_1\omega_n \tan(\omega_1 T) = 0 \quad (37)$$

The critical value of d is then computed from $|G(i\omega_1)| = 1$, or

$$d = \frac{\omega_n}{2\zeta\omega_1^2 \sqrt{1 + \tan^2(\omega_1 T)}} \quad (38)$$

Steady-state bifurcations

As was mentioned in the section on critical preview distance, it is not possible for this system to experience multiple equilibrium states or steady-state bifurcations unlike the dive plane case studied in Papoulias (1992b). In this section we show that this is directly related to the existence of hydrostatic restoring moments. Consider the system

$$\dot{\psi} = r, \quad \dot{r} = ar + a_1\psi + b\delta_{\text{sat}} \tanh\left(\frac{\delta_0}{\delta_{\text{sat}}}\right) \quad (39)$$

where a_1 represents a linearized hydrostatic restoring moment coefficient. If the heading system is characterized through its natural frequency ω_n and damping ratio ζ , the gains in the control law (7) are given by

$$k_1 = -\frac{a_1 + \omega_n^2}{b}, \quad k_2 = -\frac{a + 2\zeta\omega_n}{b}$$

Pursuit guidance is then obtained through equations (14) and (15) as before. The characteristic equation of the combined guidance and control system is then

$$s^3 - 2\zeta\omega_n s^2 - \omega_n^2 s + \frac{a_1 + \omega_n^2}{d} = 0 \quad (40)$$

Loss of stability of equation (40) occurs at

$$d = \frac{a_1 + \omega_n^2}{2\zeta\omega_n^3} \quad (41)$$

when a pair of complex conjugate roots of (40) crosses the imaginary axis, or at

$$a_1 + \omega_n^2 = 0 \quad \text{or} \quad k_1 = 0 \quad (42)$$

when a real root of (40) crosses zero. Conditions (41) and (42) cannot occur simultaneously since this would suggest $d = 0$ which is physically not realizable.

The resulting steady state when k_1 crosses zero is characterized by $\psi = \text{const.}$, $r = 0$, and $\dot{y} = \text{const.}$; i.e., linearly increasing path deviation in time, and it can be shown to be asymptotically stable regardless of the value of the preview distance d (Papoulias 1993b). In view of (42) it can be seen that this divergent instability is possible only if $a_1 < 0$, or when the hydrostatic restoring moment is stabilizing. For horizontal plane motions this might occur in cases like that of a vehicle propelled via a tether. In cases where a hydrostatic restoring moment is either nonexistent or destabilizing (wall proximity effects, for example), the above form of instability cannot occur.

3. Bifurcations to periodic solutions

As the preview distance d crosses the critical value (22), one pair of complex conjugate eigenvalues of the linearized system matrix (20) crosses transversally the imaginary axis. In this generic Poincaré-Andronov-Hopf (PAH) bifurcation a family of periodic solutions coexists with the stable/unstable nominal equilibrium state. Locally, as d approaches d_{crit} , the above periodic solutions are located on the two-dimen-

sional Euclidean plane spanned by the eigenvectors of (20) which correspond to the critical pair of eigenvalues. In order to establish the stability properties of these periodic solutions first we proceed as follows:

- Isolate the main nonlinear terms that dominate the dynamics of (18).
- Rewrite the system of equations in its normal coordinate form.
- Use the center manifold theorem to reduce the system into a two-dimensional system.
- Apply the method of averaging on the reduced system.
- Introduce polar coordinates on the averaged system to reveal the existence of limit cycles.

Third-order expansions

System (18) is written in the form

$$\dot{\mathbf{x}} = \mathbf{A}\mathbf{x} + \mathbf{g}(\mathbf{x}) \quad (43)$$

where

$$\mathbf{A} = \begin{bmatrix} 0 & 1 & 0 \\ -\omega_n^2 & -2\zeta\omega_n & -\frac{\omega_n^2}{d} \\ 1 & 0 & 0 \end{bmatrix} \quad (44)$$

and $\mathbf{g}(\mathbf{x})$ contains all nonlinear terms of equations (17). We expand $\mathbf{g}(\mathbf{x})$ in a Taylor series in \mathbf{x} and we keep the first non-vanishing coefficients only. Due to the port/starboard symmetry of the equations, the second-order terms in the Taylor expansion of $\mathbf{g}(\mathbf{x})$ automatically vanish, and we get

$$\dot{\mathbf{x}} = \mathbf{A}\mathbf{x} + \mathbf{g}^{(3)}(\mathbf{x}) \quad (45)$$

where $\mathbf{g}^{(3)}(\mathbf{x})$ contains third-order terms only

$$\begin{aligned} g_1^{(3)} &= 0 \\ g_2^{(3)} &= -\frac{b}{3\delta_{\text{sat}}^2} \delta_0^3 \\ g_3^{(3)} &= -\frac{1}{6} \psi^3 \end{aligned} \quad (46)$$

The δ_0^3 term in (46) is computed as

$$\begin{aligned} \delta_0^3 &= \left(k_1\psi + k_2r + k_1 \tan^{-1} \frac{y}{d} \right)^3 \\ &= \left(k_1\psi + k_2r + \frac{k_1}{d}y - \frac{k_1}{3d^3}y^3 \right)^3 \\ &= k_1^3\psi^3 + k_2^3r^3 + 3k_1^2k_2\psi^2r + 3k_1k_2^2\psi r^2 + \frac{k_1^3}{d^3}y^3 + 3\frac{k_1^3}{d}\psi^2y \\ &\quad + 3\frac{k_1k_2^2}{d}r^2y + 6\frac{k_1^2k_2}{d}\psi r y + 3\frac{k_1^3}{d^2}\psi y^2 + 3\frac{k_1^2k_2}{d^2}r y^2 \end{aligned}$$

where terms higher than third-order have been eliminated.

Coordinate transformations

At the bifurcation point $d = 1/2\zeta\omega_n$, matrix \mathbf{A} has the eigenvalues

$$\lambda_1 = -\omega_n i, \quad \lambda_2 = \omega_n i, \quad \lambda_3 = -2\zeta\omega_n \quad (47)$$

If we introduce the transformation matrix

$$\mathbf{T} = \begin{bmatrix} 1 & 0 & 1 \\ 0 & -\omega_n & -2\zeta\omega_n \\ 0 & \frac{1}{\omega_n} & -\frac{1}{2\zeta\omega_n} \end{bmatrix}$$

the transformation

$$\mathbf{x} = \mathbf{T}\mathbf{z}, \quad \dot{\mathbf{z}} = \mathbf{T}^{-1}\dot{\mathbf{x}} \quad (48)$$

transforms system (45) into its normal coordinate form

$$\dot{\mathbf{z}} = \mathbf{T}^{-1}\mathbf{A}\mathbf{T}\mathbf{z} + \mathbf{T}^{-1}\mathbf{g}^{(3)}(\mathbf{T}\mathbf{z}) \quad (49)$$

where

$$\mathbf{T}^{-1} = \frac{2\zeta}{4\zeta^2 + 1} \begin{bmatrix} \frac{4\zeta^2 + 1}{2\zeta} & \frac{1}{\omega_n} & \omega_n \\ 0 & -\frac{1}{2\zeta\omega_n} & 2\zeta\omega_n \\ 0 & -\frac{1}{\omega_n} & -\omega_n \end{bmatrix}$$

and

$$\mathbf{T}^{-1}\mathbf{A}\mathbf{T} = \begin{bmatrix} 0 & -\omega_n & 0 \\ \omega_n & 0 & 0 \\ 0 & 0 & -2\zeta\omega_n \end{bmatrix}$$

The relation between the physical variables ψ , r , y , and the transformed variables z_1 , z_2 , z_3 follows from (48)

$$\begin{aligned} \psi &= z_1 + z_3 \\ r &= -\omega_n z_2 - 2\zeta\omega_n z_3 \\ y &= \frac{1}{\omega_n} z_2 - \frac{1}{2\zeta\omega_n} z_3 \end{aligned} \quad (50)$$

The coordinate z_3 corresponds to the negative eigenvalue λ_3 and, therefore, the flow of (43) in the direction of z_3 converges to zero. All interesting bifurcation phenomena are locally restricted on a two-dimensional manifold that describes the time evolution of the critical coordinates z_1 , z_2 ; this is the center manifold of (43). According to the center manifold theorem (Guckenheimer & Holmes 1983), the stable coordinate z_3 can be expressed as a function of the critical coordinates z_1 , z_2 , and this relationship is at least of quadratic order. Therefore, z_3 does not affect the third-order expansions in (49), and we can write

$$\psi = z_1, \quad r = -\omega_n z_2, \quad y = \frac{1}{\omega_n} z_2 \quad (51)$$

Substitution of (51) into (49) results in

$$\dot{z}_1 = -\omega_n z_2 + r_{11}z_1^3 + r_{12}z_1^2z_2 + r_{13}z_1z_2^2 + r_{14}z_2^3 \quad (52)$$

$$\dot{z}_2 = +\omega_n z_1 + r_{21}z_1^3 + r_{22}z_1^2z_2 + r_{23}z_1z_2^2 + r_{24}z_2^3 \quad (53)$$

which describes the suspended flow of (49) on its center manifold. Expressions for the terms r_{ij} in (52) and (53) are computed from (46) and (51) at the bifurcation point $d = 1/2\zeta\omega_n$, and are presented at the end of this section.

For values of d close to its critical value, equations (52) and (53) become

$$\dot{z}_1 = \alpha'\epsilon z_1 - (\omega_n + \omega'\epsilon)z_2 + r_{11}z_1^3 + r_{12}z_1^2z_2 + r_{13}z_1z_2^2 + r_{14}z_2^3 \quad (54)$$

$$\dot{z}_2 = (\omega_n + \omega'\epsilon)z_1 + \alpha'\epsilon z_2 + r_{21}z_1^3 + r_{22}z_1^2z_2 + r_{23}z_1z_2^2 + r_{24}z_2^3 \quad (55)$$

where ϵ is the difference between d and d_{crit} ,

$$d = \frac{1}{2\zeta\omega_n} + \epsilon \quad (56)$$

The terms α' (ω') denote the derivative of the real (imaginary) part of the critical pair of eigenvalues with respect to d evaluated at $d = d_{crit}$, and are computed from a perturbation series approach as follows. The characteristic equation of (44) is

$$\lambda^3 + 2\zeta\omega_n\lambda^2 + \omega_n^2\lambda + \frac{\omega_n^2}{d} = 0 \quad (57)$$

and using (56) this is written as

$$\lambda^3 + 2\zeta\omega_n\lambda^2 + \omega_n^2\lambda + 2\zeta\omega_n^3(1 - 2\epsilon\zeta\omega_n) = 0 \quad (58)$$

where terms of order ϵ^2 and higher have been neglected. The eigenvalues of (58) are expressed as

$$\lambda_{2,3} = \alpha'\epsilon \mp (\omega_n + \omega'\epsilon)i \quad (59)$$

Substitution of (59) into (58) yields

$$\alpha' = -\frac{2\zeta^2\omega_n^2}{4\zeta^2 + 1} \quad (60)$$

$$\omega' = -\frac{4\zeta^3\omega_n^2}{4\zeta^2 + 1} \quad (61)$$

With these last two expressions, the center manifold reduction of our system in the form of (54) and (55) is complete.

Finally, the expressions for the r_{ij} terms in (54) and (55) are

$$r_{11} = -\frac{2\zeta\omega_n}{4\zeta^2 + 1} \left(-\frac{\omega_n^4}{3\delta_{sat}^2 b^2} + \frac{1}{6} \right)$$

$$r_{12} = -\frac{2\zeta\omega_n^4 a}{\delta_{sat}^2 b^2 (4\zeta^2 + 1)}$$

$$r_{13} = \frac{2\zeta\omega_n^3 a^2}{\delta_{sat}^2 b^2 (4\zeta^2 + 1)}$$

$$r_{14} = -\frac{2\zeta\omega_n^2 a^3}{3\delta_{sat}^2 b^2 (4\zeta^2 + 1)}$$

$$r_{21} = \frac{-2\zeta\omega_n}{3(4\zeta^2 + 1)} \left(\zeta + \frac{\omega_n^4}{2\zeta\delta_{sat}^2 b^2} \right)$$

$$r_{22} = \frac{\omega_n^4 a}{\delta_{sat}^2 b^2 (4\zeta^2 + 1)}$$

$$r_{23} = -\frac{\omega_n^3 a^2}{\delta_{sat}^2 b^2 (4\zeta^2 + 1)}$$

$$r_{24} = \frac{\omega_n^2 a^3}{3\delta_{sat}^2 b^2 (4\zeta^2 + 1)}$$

Averaging

We write equations (54) and (55) in the form

$$\dot{z}_1 = \alpha'\epsilon z_1 - (\omega_n + \omega'\epsilon)z_2 + F_1(z_1, z_2) \quad (62)$$

$$\dot{z}_2 = (\omega_n + \omega'\epsilon)z_1 + \alpha'\epsilon z_2 + F_2(z_1, z_2) \quad (63)$$

where the F_1, F_2 functions contain the third-order expansion

terms. These are evaluated at $\epsilon = 0$ since terms of the form ϵz_i^3 are higher order compared to z_i^3 and can be neglected. If we introduce polar coordinates in the form

$$z_1 = R \cos \theta, \quad z_2 = R \sin \theta \quad (64)$$

equations (62) and (63) are written as

$$\begin{aligned} \dot{R} &= \alpha'\epsilon R + F_1(R \cos \theta, R \sin \theta) \cos \theta \\ &\quad + F_2(R \cos \theta, R \sin \theta) \sin \theta \end{aligned} \quad (65)$$

$$\begin{aligned} R\dot{\theta} &= (\omega_n + \omega'\epsilon)R + F_2(R \cos \theta, R \sin \theta) \cos \theta \\ &\quad - F_1(R \cos \theta, R \sin \theta) \sin \theta \end{aligned} \quad (66)$$

Equation (65) is written in the form

$$\dot{R} = \alpha'\epsilon R + \mathcal{P}(\theta)R^3 \quad (67)$$

where the function $\mathcal{P}(\theta)$ is 2π -periodic in the angular coordinate θ

$$\begin{aligned} \mathcal{P}(\theta) &= r_{11} \cos^4 \theta + r_{12} \cos^3 \theta \sin \theta + r_{13} \cos^2 \theta \sin^2 \theta \\ &\quad + r_{14} \cos \theta \sin^3 \theta + r_{21} \cos^3 \theta \sin \theta + r_{22} \cos^2 \theta \sin^2 \theta \\ &\quad + r_{23} \cos \theta \sin^3 \theta + r_{24} \sin^4 \theta \end{aligned}$$

If equation (67) is averaged over one cycle in θ , we get an equation with constant coefficients

$$\dot{R} = \alpha'\epsilon R + \mathcal{H}R^3 \quad (68)$$

where

$$\mathcal{H} = \frac{1}{2\pi} \int_0^{2\pi} \mathcal{P}(\theta) d\theta \quad (69)$$

Evaluating the integral in (69) we get

$$\mathcal{H} = \frac{1}{8} (3r_{11} + r_{13} + r_{22} + 3r_{24})$$

and using the values for r_{ij} ,

$$\mathcal{H} = \frac{-\zeta\omega_n\delta_{sat}^2 b^2 + \omega_n^2(\omega_n^2 + a^2)(2\zeta\omega_n + a)}{8\delta_{sat}^2 b^2 (4\zeta^2 + 1)} \quad (70)$$

Similar averaging can be performed for equation (66) which has the form

$$\dot{\theta} = \omega_n + \omega'\epsilon + \mathcal{F}(\theta)R^2 \quad (71)$$

where

$$\begin{aligned} \mathcal{F}(\theta) &= r_{21} \cos^4 \theta + r_{22} \cos^3 \theta \sin \theta + r_{23} \cos^2 \theta \sin^2 \theta \\ &\quad + r_{24} \cos \theta \sin^3 \theta - r_{11} \cos^3 \theta \sin \theta - r_{12} \cos^2 \theta \sin^2 \theta \\ &\quad - r_{13} \cos \theta \sin^3 \theta - r_{14} \sin^4 \theta \end{aligned}$$

and we have assumed $R \neq 0$. The averaged form of (71) is

$$\dot{\theta} = \omega_n + \omega'\epsilon + \mathcal{M}R^2 \quad (72)$$

where

$$\mathcal{M} = \frac{1}{2\pi} \int_0^{2\pi} \mathcal{F}(\theta) d\theta = \frac{1}{8} (3r_{21} + r_{23} - r_{12} - 3r_{14})$$

and using the values for r_{ij} ,

$$\mathcal{M} = \frac{2\zeta^2\omega_n^3\delta_{sat}^2 b^2 + \omega_n^2(\omega_n^2 + a^2)(2\zeta a - \omega_n)}{8\delta_{sat}^2 b^2 (4\zeta^2 + 1)} \quad (73)$$

Limit cycle analysis

Equation (68) has two steady-state solutions, one at $R = 0$ which corresponds to the trivial equilibrium solution at zero, and one at

$$R_0^2 = -\frac{\alpha'}{\mathcal{H}} \epsilon \quad (74)$$

This equilibrium solution corresponds to a periodic solution or limit cycle in the Cartesian coordinates z_1, z_2 from (64). Since α' as seen by (60) is always negative, existence of these periodic solutions depends on the value of K . Specifically,

- if $\mathcal{H} < 0$, periodic solutions exist for $\epsilon < 0$ or $d < d_{crit}$, and
- if $\mathcal{H} > 0$, periodic solutions exist for $\epsilon > 0$ or $d > d_{crit}$.

The Floquet exponent of (68) in the vicinity of (74) is

$$\beta = -2\alpha'\epsilon \quad (75)$$

and we can see that

- if periodic solutions exist for $d < d_{crit}$ they are stable, and
- if periodic solutions exist for $d > d_{crit}$ they are unstable.

We refer to the first case as the supercritical PAH bifurcation and to the second case as the subcritical PAH bifurcation.

The period of these limit cycles is computed by substituting (74) in (72),

$$T = \frac{2\pi}{\omega_n + \omega'\epsilon + MR_0^2} = \frac{2\pi}{\omega_n} \left(1 - \frac{\omega'\mathcal{H} - \alpha'M}{\omega_n\mathcal{H}} \epsilon \right) + O(\epsilon^2) \quad (76)$$

The amplitude of the limit cycles is computed from (74) and (64), and in terms of the path deviation y which is the most important physical parameter in our problem, we have

$$y = \frac{1}{\omega_n} R_0 = \frac{1}{\omega_n} \left(-\frac{\alpha'}{\mathcal{H}} \epsilon \right)^{1/2} \quad (77)$$

We can see that in the supercritical case, on loss of stability of equilibrium the steady state becomes a periodic oscillatory state, the amplitude of the oscillation being proportional to the square root of the criticality ϵ , the difference of the preview distance from the critical value at which stability of equilibrium is lost. This form of loss of stability is called "soft" loss of stability since the oscillating state for small ϵ differs little from the equilibrium state. In the subcritical case, before the steady state loses stability the domain of attraction becomes very small as is bounded by the amplitudes of the unstable limit cycles, and a random disturbance can throw the system off its equilibrium state even before its domain of attraction has completely disappeared. This form of loss of stability is called "hard". Here the system leaves its steady state with a jump to a different state of motion which in our case is most likely to be a stable oscillation with a locally discontinuous increase in the amplitude.

For supercritical PAH bifurcations $\mathcal{H} < 0$, we must have

$$\zeta \leq \zeta_{crit} \quad (78)$$

where ζ_{crit} is evaluated from $\mathcal{H} = 0$, or

$$\zeta_{crit} = \frac{\omega_n a (\omega_n^2 + a^2)}{\delta_{sat}^2 b^2 - 2\omega_n^2 (\omega_n^2 + a^2)} \quad (79)$$

Numerical results

A plot of the critical preview distance d_{crit} from (22) versus ω_n and with the damping ratio ζ as the parameter is shown

in Fig. 3. For higher values of ω_n the heading autopilot becomes more responsive as evidenced from the expressions for the gains (11) and (12). As a result, it is possible to tolerate smaller values of d without loss of stability of straight line motion. For the bifurcation points of Fig. 3, the corresponding values of the cubic coefficient K are shown in Fig. 4 versus ω_n for different values of ζ and for $\delta_{sat} = 0.4$ radians. It can be seen that for lower values of ω_n (softer control law), the corresponding PAH bifurcations are supercritical while they become subcritical for ω_n beyond a critical value. Similar results hold for a fixed ω_n and varying damping ratios ζ . The effects of the saturation level δ_{sat} are shown in Fig. 5 where \mathcal{H} is presented versus ω_n for $\zeta = 0.7$ and different values of δ_{sat} . It can be seen that although δ_{sat} has no effect on initial loss of stability of straight-line motion, it is directly related to the nominal state's domain of attraction and the stability of the resulting limit cycles. As $\delta_{sat} \rightarrow \infty$ all PAH bifurcations are supercritical as is also seen from equation (70). The critical value of ζ , ζ_{crit} , for transition between supercritical and subcritical bifurcations is presented in Fig. 6 and is increasing for increasing δ_{sat} or decreasing ω_n .

Theoretical predictions of stable and unstable limit cycles are verified in Figs. 7 through 9 from direct numerical integrations of the equations of motion (17). Results in terms of the path deviation y versus d for $\zeta = 0.5$, $\omega_n = 1$, and $\delta_{sat} = 0.4$, are shown in Fig. 7 where a solid line corresponds to a stable, and a dotted line to an unstable attractor. The nominal straight-line motion loses its stability for $d_{crit} = 1$ and the amplitudes of the stable steady-state periodic motions are plotted versus d . Equation (77) predicts for this case

$$y = 1.57(d_{crit} - d)^{1/2} + O(d_{crit} - d)$$

which agrees qualitatively with the simulated envelope of Fig. 7. For $d = 0.9$ the estimated limit cycle amplitude is 0.5 versus the exact 0.55. For $\omega_n = 4$ which results in $\mathcal{H} > 0$ and therefore subcritical bifurcations, the corresponding numerical integration results are shown in Fig. 8. The dotted curves in the figure correspond to unstable limit cycle amplitudes and numerically they were established by an iterative shooting scheme; the initial conditions in y were systematically varied for convergence to either zero or periodic motion. The existence of these unstable limit cycles limits the domain of attraction of the nominal motion for $d > d_{crit}$ as shown in Fig. 9. The results of three numerical integrations are presented in the (y, \dot{y}) subphase plot for $d = 0.4$ along with the unstable limit cycle in the dotted curve. The unstable limit cycle was established here as the outer en-

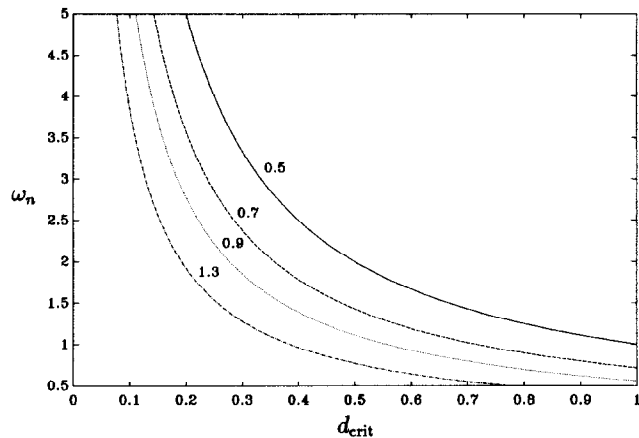


Fig. 3 Critical preview distance versus ω_n , for different values of ζ

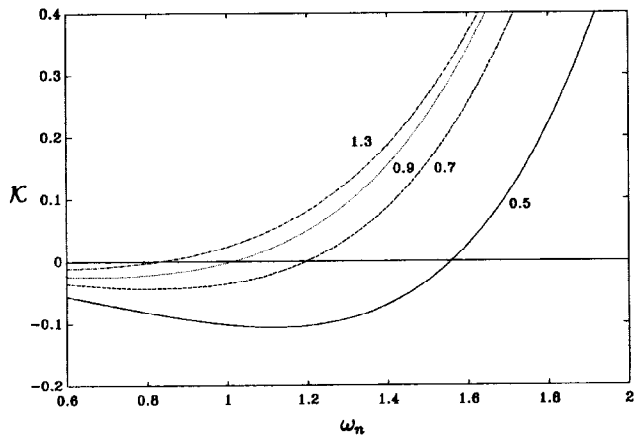


Fig. 4 Cubic coefficient K versus ω_n for $\delta_{sat} = 0.4$ and different values of ζ

velope of those (y, \dot{y}) initial conditions that resulted in convergence to zero. Convergence to zero is ensured only for initial conditions that lie inside the unstable limit cycle. A rather slow convergence to the stable limit cycle is observed for initial conditions that lie between the unstable and stable limit cycles; this is due to the opposing directions of attraction of

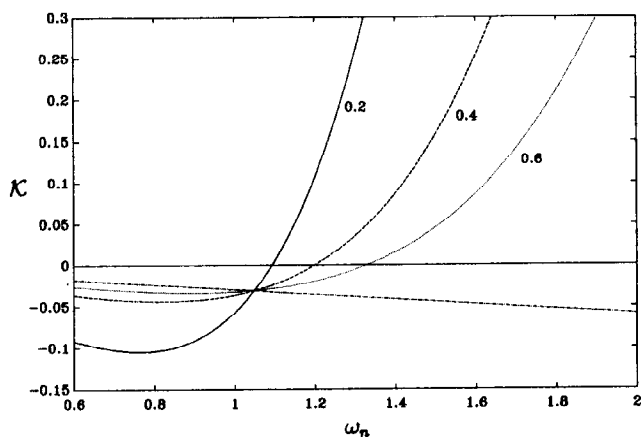


Fig. 5 Cubic coefficient K versus ω_n for $\zeta = 0.7$ and different values of δ_{sat}

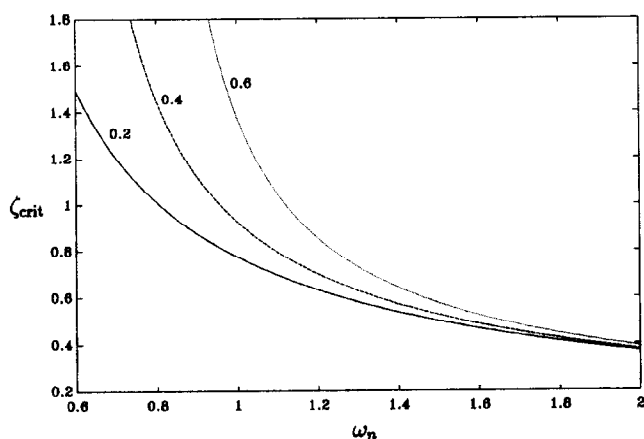


Fig. 6 Critical damping ratio versus ω_n for different values of δ_{sat}

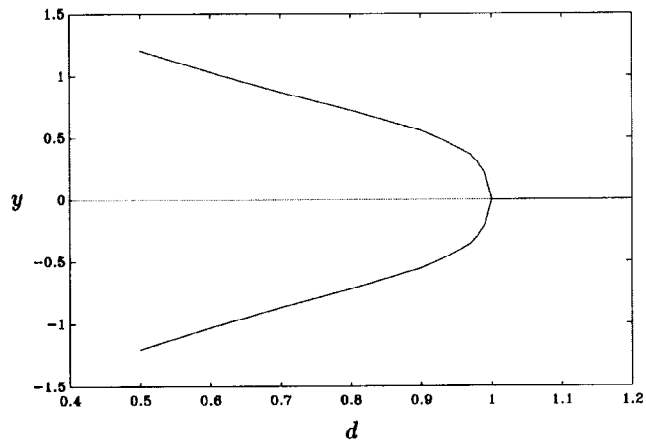


Fig. 7 Stable and unstable limit sets for $\zeta = 0.5$ and $\omega_n = 1$

the stable equilibrium and the stable limit cycle. Fast convergence to the stable limit cycle is observed for initial conditions that lie outside its envelope; this is because in this case both stable equilibrium and limit cycle attract state trajectories in the same direction. The amplitude of the unstable limit cycle was established at $y = 0.08$ from Fig. 9, while equation (77) predicts a value of $y = 0.085(d - d_{crit})^{1/2}$, or $y = 0.033$. The agreement is not as good as for the Fig. 7 case, and this is due to the higher difference between d and d_{crit} considered here. The agreement between simulated and predicted results becomes better as d approaches the critical value d_{crit} .

Fifth-order approximations

Transitions between supercritical and subcritical PAH bifurcations can only be analyzed by incorporating fifth-order terms in our previous Taylor series expansions. To this end, we use

$$\sin \psi = \psi - \frac{1}{6} \psi^3 + \frac{1}{120} \psi^5$$

$$\delta = \delta_0 - \frac{1}{3\delta_{sat}^2} \delta_0^3 + \frac{2}{15\delta_{sat}^4} \delta_0^5$$

$$\delta_0 = k_1 \psi + k_2 r + \frac{k_1}{d} y - \frac{k_1}{3d^3} y^3 + \frac{k_1}{5d^5} y^5$$

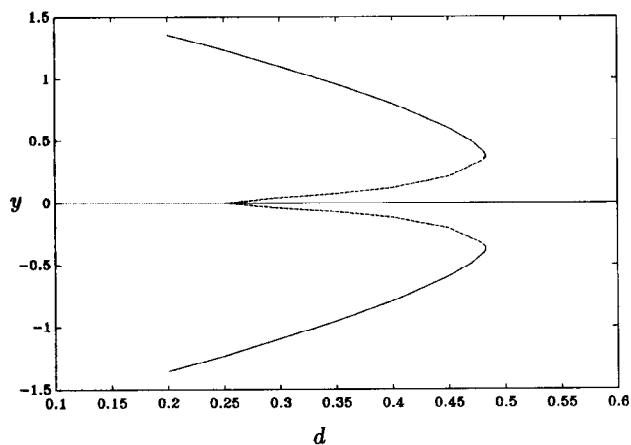


Fig. 8 Stable and unstable limit sets for $\zeta = 0.5$ and $\omega_n = 4$

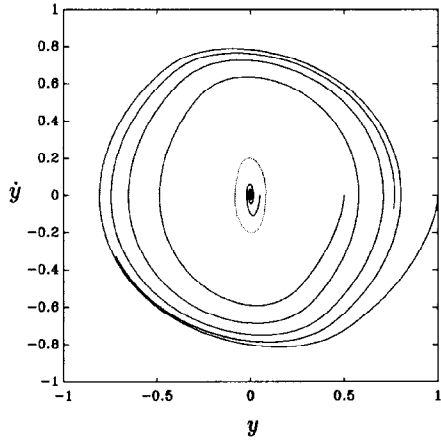


Fig. 9 Convergence to stable equilibrium and stable limit cycle for $\zeta = 0.5$, $\omega_n = 4$, and $d = 0.4$

in the equations of motion (18) and we neglect terms of order higher than five. The transformation matrix \mathbf{T} is used as in (48) to transform the system into its normal coordinate form. This procedure yields

$$\dot{z}_1 = -\omega_n z_2 + n_{12} h_2 + n_{13} h_3 + n_{12} h_2^c + n_{13} h_3^c \quad (80)$$

$$\dot{z}_2 = +\omega_n z_1 + n_{22} h_2 + n_{23} h_3 + n_{22} h_2^c + n_{23} h_3^c \quad (81)$$

for $d = d_{crit}$. The terms n_{ij} represent the elements of \mathbf{T}^{-1} , and the functions h_2, h_3 contain the third- and fifth-order expansion terms in z_1, z_2

$$\begin{aligned} h_2 = & -\frac{\omega_n^3}{3\delta_{sat}^2 b^2} (-\omega_n^3 z_1^3 + 3\omega_n^2 a z_1^2 z_2 - 3\omega_n a^2 z_1 z_2^2 + a^3 z_2^3) \\ & + 8\omega_n^3 \zeta^3 z_1^2 z_2^3 + 8\omega_n \zeta^3 a^2 z_2^5 - 32\omega_n^3 \zeta^4 z_1 z_2^4 \\ & + \frac{2\omega_n^5}{15\delta_{sat}^4 b^4} (-\omega_n^5 z_1^5 - 10\omega_n^3 a^2 z_1^3 z_2^2 + 10\omega_n^2 a^3 z_1^2 z_2^3 \\ & + 5\omega_n^4 a z_1^4 z_2 - 5\omega_n a^4 z_1 z_2^4 + a^5 z_2^5) \\ h_3 = & -\frac{1}{6} z_1^3 + \frac{1}{120} z_1^5 \end{aligned}$$

where substitutions (51) were used. The key behind these substitutions is the center manifold theorem which ensures that the stable coordinate z_3 is at least of quadratic order in terms of z_1, z_2 . In our case, because of the symmetry of the problem, z_3 is at least of cubic order in z_1, z_2 . Therefore, in general we can say that

$$z_3 = \alpha_1 z_1^3 + \alpha_2 z_2^3 + \alpha_3 z_1^2 z_2 + \alpha_4 z_1 z_2^2 \quad (82)$$

which supplies a local approximation of the center manifold as a function of the four unknown coefficients α_i . Equation (82) simplified the third-order expansion analysis considerably since it allowed use of (51) instead of (50). This is no longer possible when we consider fifth-order terms and it is easy to see that terms of the form $z_1^2 z_3, z_2^2 z_3$, and $z_1 z_2 z_3$, will be of fifth-order in z_1, z_2 and they will generate contributions in the expansions (80) and (81). These extra terms are designated by h_2^c, h_3^c since they arise from the center manifold expansion (82) and are given by

$$\begin{aligned} h_2^c = & -\frac{2\omega_n^3 \zeta (a + 2\zeta \omega_n)}{\delta_{sat}^2 b^2} [\alpha_1 \omega_n^2 z_1^5 + (\alpha_3 \omega_n - 2\alpha_1 a) \omega_n z_1^4 z_2 \\ & + (\alpha_4 \omega_n^2 + \alpha_1 a^2 - 2\alpha_3 a \omega_n) z_1^3 z_2^2 + (\alpha_2 \omega_n^2 + \alpha_3 a^2 - 2\alpha_4 \omega_n a) z_1^2 z_2^3 \\ & + (\alpha_4 a - 2\alpha_2 \omega_n) a z_1 z_2^4 + \alpha_2 a^2 z_2^5] \\ h_3^c = & -\frac{1}{2} (\alpha_1 z_1^5 + \alpha_2 z_1^2 z_2^3 + \alpha_3 z_1^4 z_2 + \alpha_4 z_1^3 z_2^2) \end{aligned}$$

In this way we arrive at the expanded form of equations (80) and (81),

$$\begin{aligned} \dot{z}_1 = & -\omega_n z_2 + \beta_{30} z_1^3 + \beta_{21} z_1^2 z_2 + \beta_{12} z_1 z_2^2 + \beta_{03} z_2^3 + \beta_{05} z_1^5 \\ & + \beta_{41} z_1^4 z_2 + \beta_{32} z_1^3 z_2^2 + \beta_{23} z_1^2 z_2^3 + \beta_{14} z_1 z_2^4 + \beta_{05} z_2^5 \quad (83) \end{aligned}$$

$$\begin{aligned} \dot{z}_2 = & +\omega_n z_1 + \gamma_{30} z_1^3 + \gamma_{21} z_1^2 z_2 + \gamma_{12} z_1 z_2^2 + \gamma_{03} z_2^3 + \gamma_{05} z_1^5 \\ & + \gamma_{41} z_1^4 z_2 + \gamma_{32} z_1^3 z_2^2 + \gamma_{23} z_1^2 z_2^3 + \gamma_{14} z_1 z_2^4 + \gamma_{05} z_2^5 \quad (84) \end{aligned}$$

where the coefficients β_{ij}, γ_{ij} are computable from the previous expressions.

The unknown coefficients in the center manifold expansion (82) can be computed as follows: Equation (82) is differentiated

$$\begin{aligned} \dot{z}_3 = & 3\alpha_1 z_1^2 \dot{z}_1 + 3\alpha_2 z_2^2 \dot{z}_2 + \alpha_3 z_1^2 \dot{z}_2 + 2\alpha_3 z_1 z_2 \dot{z}_1 \\ & + \alpha_4 z_2^2 \dot{z}_1 + 2\alpha_4 z_1 z_2 \dot{z}_2 \quad (85) \end{aligned}$$

Equations (49) can be used in the form

$$\begin{aligned} \dot{z}_1 = & -\omega_n z_2 \\ \dot{z}_2 = & +\omega_n z_1 \\ \dot{z}_3 = & -2\zeta \omega_n z_3 + C_{300} z_1^3 + C_{030} z_2^3 + C_{210} z_1^2 z_2 + C_{120} z_1 z_2^2 \quad (86) \end{aligned}$$

where

$$\begin{aligned} C_{300} = & \frac{\zeta \omega_n}{3(4\zeta^2 + 1)} - \frac{2\zeta \omega_n^5}{3(4\zeta^2 + 1)\delta_{sat}^2 b^2} \\ C_{030} = & \frac{2\zeta \omega_n^2 a^3}{3(4\zeta^2 + 1)\delta_{sat}^2 b^2} \\ C_{210} = & -\frac{2\zeta \omega_n^3 a^2}{(4\zeta^2 + 1)\delta_{sat}^2 b^2} \\ C_{120} = & \frac{2\zeta \omega_n^4 a}{(4\zeta^2 + 1)\delta_{sat}^2 b^2} \end{aligned}$$

Additional terms in (86) do not affect the computations of α_i . If we substitute (82) and (86) into (85) and equate coefficients we find

$$\begin{aligned} 2\zeta \omega_n \alpha_1 + \omega_n \alpha_3 & = C_{300} \\ 2\zeta \omega_n \alpha_2 + \omega_n \alpha_4 & = C_{030} \\ -3\omega_n \alpha_1 + 2\zeta \omega_n \alpha_3 + 2\omega_n \alpha_4 & = C_{210} \\ 3\omega_n \alpha_2 - 2\omega_n \alpha_3 + 2\zeta \omega_n \alpha_4 & = C_{120} \end{aligned}$$

Solution of this system produces the desired coefficients in the center manifold series expansion (82).

In polar coordinates the system of equations (83) and (84) becomes

$$\dot{R} = \mathcal{P}(\theta)R^3 + \mathcal{Q}(\theta)R^5 \quad (87)$$

and its averaged form is

$$\dot{R} = \mathcal{H}R^3 + \mathcal{L}R^5 \quad (88)$$

where

$$\mathcal{L} = \frac{1}{2\pi} \int_0^{2\pi} \mathcal{Q}(\theta) d\theta \quad (89)$$

Performing the indicated integration in (89) we find

$$\mathcal{L} = \frac{1}{16} (5\beta_{50} + \beta_{32} + \beta_{14} + \gamma_{41} + \gamma_{23} + 5\gamma_{05}) \quad (90)$$

where

$$\beta_{50} = -\frac{4\omega_n^4 \zeta}{(4\zeta^2 + 1)\delta_{\text{sat}}^2 b^2} \left[\frac{\omega_n^5}{15\delta_{\text{sat}}^2 b^2} + \zeta(a + 2\zeta\omega_n)\alpha_1 \right] - \frac{\zeta\omega_n}{4\zeta^2 + 1} \left(\alpha_1 - \frac{1}{60} \right)$$

$$\beta_{32} = -\frac{4\zeta\omega_n^2}{(4\zeta^2 + 1)\delta_{\text{sat}}^2 b^2} \left[\frac{2\omega_n^5 a^2}{3\delta_{\text{sat}}^2 b^2} + \zeta(a + 2\zeta\omega_n)(\alpha_4\omega_n^2 + \alpha_1 a^2 - 2\alpha_3 a\omega_n) \right]$$

$$\beta_{14} = -\frac{4\zeta\omega_n^2}{(4\zeta^2 + 1)\delta_{\text{sat}}^2 b^2} \left[-\frac{16}{3} \omega_n^3 \zeta^4 + \frac{\omega_n^3 a^4}{3\delta_{\text{sat}}^2 b^2} + \zeta(a + 2\zeta\omega_n)(\alpha_4 a - 2\alpha_2 \omega_n) a \right]$$

$$\gamma_{41} = -\frac{2\omega_n^3}{(4\zeta^2 + 1)\delta_{\text{sat}}^2 b^2} \left[\frac{\omega_n^5 a}{3\delta_{\text{sat}}^2 b^2} - \zeta(a + 2\zeta\omega_n)(\alpha_3 \omega_n - 2\alpha_1 a) \right]$$

$$\gamma_{23} = \frac{2\omega_n^2}{(4\zeta^2 + 1)\delta_{\text{sat}}^2 b^2} \left[\frac{4}{3} \omega_n^3 \zeta^3 - \frac{2\omega_n^4 a^3}{3\delta_{\text{sat}}^2 b^2} + \zeta(a + 2\zeta\omega_n)(\alpha_2 \omega_n^2 + \alpha_3 a^2 - 2\alpha_4 \omega_n a) \right]$$

$$\gamma_{05} = \frac{2\omega_n^2 a^2}{(4\zeta^2 + 1)\delta_{\text{sat}}^2 b^2} \left[\frac{4}{3} \omega_n \zeta^3 - \frac{\omega_n^2 a^3}{15\delta_{\text{sat}}^2 b^2} + \zeta(a + 2\zeta\omega_n)\alpha_2 \right]$$

A plot of the cubic coefficient \mathcal{K} and the quintic coefficient \mathcal{L} versus ω_n for $\zeta = 0.5$ and $\delta_{\text{sat}} = 0.4$ is shown in Fig. 10. The existence of a negative coefficient \mathcal{L} when \mathcal{K} is positive generates an additional stable limit cycle surrounding the unstable limit cycle of the subcritical PAH bifurcation

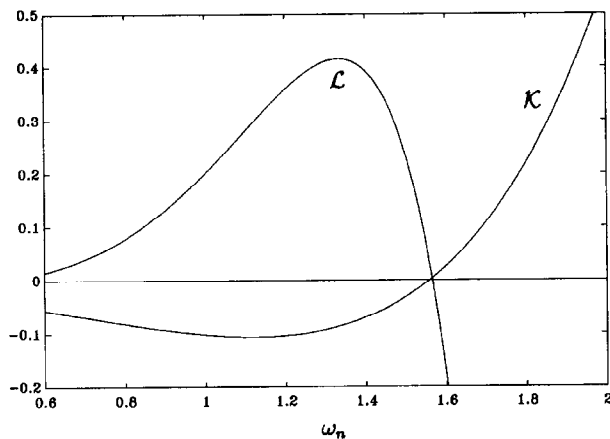


Fig. 10 Cubic coefficient \mathcal{K} and quintic coefficient \mathcal{L} versus ω_n for $\zeta = 0.5$ and $\delta_{\text{sat}} = 0.4$

(Guckenheimer & Holmes 1983). The existence of this double limit cycle was observed numerically in Figs. 8 and 9. Farther away from the bifurcation point, the $\mathcal{L}\mathcal{R}^5$ term overpowers the $\mathcal{K}\mathcal{R}^3$ term, and this causes the limit cycle amplitudes to veer to the left (i.e., decreasing values of d) and change their stability as shown in Fig. 8.

Concluding remarks

An analytic investigation of the nonlinear dynamic response characteristics of pursuit guidance coupled with orientation control law of marine vehicles has been presented. Bifurcation theory techniques were utilized in order to assess the behavior of the system upon initial loss of stability. The main bifurcation parameters were the system damping ratio, natural frequency, preview distance, and control saturation level. The main conclusions of this research are summarized as follows:

1. There exists a critical preview distance d_{crit} for stability of straight-line motion. This is inversely proportional to the product of the system damping ratio and the natural frequency. For $d < d_{\text{crit}}$ the nominal equilibrium state loses its stability and the response admits oscillatory characteristics.

2. The critical preview distance is a maximum for straight-line nominal paths and it is a monotonically decreasing function of the path radius of curvature. Thus, stability along straight-line paths guarantees stability along curved paths as well.

3. The existence of time lags in navigational positional information results in an increase in the value of d_{crit} . To first-order approximation, this increase equals the amount of time lag.

4. Stabilizing positional restoring moments, such as hydrostatic or spring constant effects, have a destabilizing effect on stability of motion of the scheme. This destabilizing effect manifests itself via a divergent type of instability. Destabilizing spring constant moments prohibit this divergent instability.

5. The occurrence of bifurcations to periodic solutions was established via a third-order expansion in the equations of motion. The method of averaging was utilized in order to predict the existence and stability characteristics of the resulting limit cycles. It was shown that for stable limit cycles to exist upon initial loss of stability of straight-line motion, the selected damping ratio for the system must be less than a certain critical value. Overdamping results in unstable limit cycles with a progressively smaller region of stability of the straight-line motion as $d \rightarrow d_{\text{crit}}$.

6. Transition between supercritical and subcritical PAH bifurcations was studied by performing a lengthy fifth-order expansion in the equations of motion. This task required a third-order approximation of the center manifold of the system at the critical point d_{crit} . The quintic coefficient of the averaged system indicated the local existence of two limit cycles, one stable and one unstable. The results were verified by direct numerical integrations.

Acknowledgments

The author would like to recognize the financial support of the Naval Postgraduate School Direct Research Fund.

References

- BAHRKE, F. 1992 On-line identification of the speed, steering and diving response parameters of an autonomous underwater vehicle from experimental data. Mechanical Engineer's thesis, Naval Postgraduate School, Monterey, Calif.
- BRUTZMAN, D. P. 1992 NPS AUV integrated simulator. M.S. thesis, Department of Computer Science, Naval Postgraduate School, Monterey, Calif.

- BYRNES, R. B., MACPHERSON, D. L., KWAK, S. H., NELSON, M. L., AND MCGHEE, R. B. 1992 An experimental comparison of hierarchical and subsumption software architectures for control of an autonomous underwater vehicle, *Proceedings, IEEE Autonomous Underwater Vehicle Conference*, Washington, D.C.
- CHOW, S.-N. AND MALLET-PARET, J. 1977 Integral averaging and bifurcation. *Journal of Differential Equations*, **26**, 112-159.
- CRANE, C. L., EDA, H., AND LANDSBURG, A. 1989 Controllability. Chapter IX in *Principles of Naval Architecture*, E. V. Lewis, Ed., SNAME, Jersey City, N.J.
- FRIEDLAND, B. 1986 *Control System Design: An Introduction to State-Space Methods*. McGraw-Hill, New York, N.Y.
- GUCKENHEIMER, J. AND HOLMES, P. 1983 *Nonlinear Oscillations, Dynamical Systems, and Bifurcations of Vector Fields*. Springer-Verlag, New York, N.Y.
- HASSARD, B. AND WAN, Y. H. 1978 Bifurcation formulae derived from center manifold theory. *Journal of Mathematical Analysis and Applications*, **63**, 297-312.
- HEALEY, A. J., MCGHEE, R. B., CRISTI, R., PAPOULIAS, F. A., KWAK, S. H., KANAYAMA, Y., AND LEE, Y. 1990 Mission planning, execution, and data analysis for the NPS AUV II autonomous underwater vehicle, *Proceedings, NSF Workshop on Mobile Undersea Robotics*, Monterey, Calif.
- KWAK, S. H., MCKEON, J. B., CLYNCH, J. R., AND MCGHEE, R. B. 1992 Incorporation of global positioning system into autonomous underwater vehicle navigation, *Proceedings, IEEE Autonomous Underwater Vehicle Conference*, Washington, D.C.
- PAPOULIAS, F. A. 1991 Stability considerations of guidance and control laws for autonomous underwater vehicles in the horizontal plane, *Proceedings, 7th International Symposium on Unmanned Untethered Submersible Technology*, Durham, N.H.
- PAPOULIAS, F. A. 1993a Loss of stability of guidance and control laws for autonomous vehicles. *Dynamics and Stability of Systems*, **8**, 1.
- PAPOULIAS, F. A. 1993b Dynamics and bifurcations of pursuit guidance for vehicle path keeping in the dive plane. *JOURNAL OF SHIP RESEARCH*, **37**, 2.
- WARNER, D. C. 1991 Design, simulation, and experimental verification of a computer model and enhanced position estimator for the NPS AUV II. Mechanical Engineer's thesis, Naval Postgraduate School, Monterey, Calif.